Assessment of MU-MIMO schemes with cylindrical arrays under 3GPP 3D channel model for B5G networks

Daniel Gaetano Riviello[1,3], Riccardo Tuninato[2,3] and Roberto Garello[2,3]

[1]Department of Electrical, Electronic, and Information Engineering (DEI), University of Bologna, Bologna, Italy
[2]Department of Electronics and Telecommunications (DET), Politecnico di Torino, Torino, Italy
[3]Consorzio Nazionale Interuniversitario per le Telecomunicazioni (CNIT), Parma, Italy
Email: daniel.riviello@unibo.it, riccardo.tuninato@polito.it, roberto.garello@polito.it

Abstract—**Beyond 5G technologies promise groundbreaking advances on the performance of cellular networks, by taking advantage of Massive MIMO in mmWave scenarios. The aim of this study is to analyze and test the performance of a 5G cell site equipped with large antenna arrays. It is of particular interest the comparison between the typical trisector cell design with a planar array for each sector, and the less investigated cylindrical array, able to maintain a constant pattern through the whole azimuthal range. To validate our analysis, we adopt the latest 3GPP-compliant 3D channel model and we evaluate the performance of multi-user and multi-layer precoding and combining schemes. Several MIMO configurations are taken into account, and we show that cylindrical arrays can improve the overall system performance, both in terms of achievable per-user rate and outage probability.**

Index Terms—**MU-MIMO, cylindrical arrays, planar arrays, precoding, mmWave, B5G.**

I. Introduction

OVER the past decade, the number of devices connected to the global network has skyrocketed, as have the number of services with increasing data requirements. To meet these new demands, the new standard for mobile networks, 5G, identifies new advanced solutions to be adopted. One of the most promising is the transition from Multiple Input Multiple Output (MIMO) systems to Massive MIMO systems, which will become available through the new bands at higher frequencies, such as the millimeter wave (mmWave) range [1]. The potential of MIMO systems is already known, but in-depth studies need to be conducted for the particular scenarios in which 5G and beyond systems will operate. The use of new appropriate channel models must be considered because, unlike LTE, the assumption of 2D propagating waves is no longer valid: the channel models must be 3D. Based on these channel models, extensive simulations can be performed to study the behavior of new techniques and technologies.

To efficiently exploit the richness of environments in which cellular networks are deployed, antenna arrays play a crucial role. In Massive MIMO systems, these antenna arrays can reach very large number of antenna elements given the very small size of each element. Moreover, different shapes and arrangements of the elements are possible, which may lead to improvements in the overall system performance. Antenna arrays are especially suited for their capability of serving multiple users simultaneously while suppressing the interference, and to put in place Spatial Division Multiple Access (SDMA) [2].

The focus of this work is on the comparison between the well-known and widely used planar arrays and the cylindrical arrays at the transmitter side, i.e., the Base Station (BS), considering a downlink (DL) scenario. In previous works [3], [4] we performed a preliminary analysis of cylindrical arrays with a simplified directive channel model, and, while other studies have investigated MIMO performance over cylindrical arrays [5], [6], to the best of the authors' knowledge, no studies have analyzed the performance of such arrays for 5G Massive MIMO in conjunction with a realistic channel model, such as the most recent implementation of the 3GPP TR 38.901 spatial channel model [7], [8].

The goal of providing SDMA requires proper precoding and combining schemes. Many precoders to separate the users have been studied in the literature, as zero-forcing [9] and Minimum Mean Square Error (MMSE) [10]. Another very effective scheme, called Signal-to-Leakage plus Noise Ratio (SLNR) technique [11] is adopted in our work. MMSE is instead implemented at the receiver side for the combiner [12], to exploit the antenna arrays of the User Terminals (UTs) and offer multi-layer capabilities.

The paper is organized as follows: Sec. II describes the scenario, Sec. III illustrates the mathematical framework for planar and cylindrical arrays, Sec. IV briefly summarizes the adopted 3GPP spatial channel model, in Sec. V-A the Multi-User Multi-Layer MIMO scheme based on SLNR precoding and MMSE combining is presented. Simulation results are discussed in Sec. VI and finally Sec. VII draws the conclusions.

II. Scenario description

We consider a cellular MIMO-OFDM network in which a single Base Station (BS) communicates with multiple outdoor User Terminals (UTs) over a wideband mmWave channel with Q subcarriers. Our analysis is carried out at system level on a subband basis. The carrier frequency f_c is set to 28 GHz.

The adopted scenario is a single circular cell in a Urban Micro (UMi) street canyon environment [7]. The Base Station (BS) can adopt Uniform Cylindrical Arrays (UCyA) or Uniform Planar Arrays (UPA), and it is placed at the center of the cell, with an height $h_{BS} = 10$ m. In case of UPA, the cell is divided into three sectors, each one served by a different UPA, while no sectorization is needed for UCyA. The area $\mathcal{A}$ occupied by the circular cell is given by $\mathcal{A} = \pi R^2$, with R the radius (by default set to 100 m). The UEs are randomly placed in $\mathcal{A}$ following a spatial homogeneous Poisson point Process. The probability of K users existing in $\mathcal{A}$ is:

$$\Pr[M(\mathcal{A}) = K] = \frac{(\mu \mathcal{A})^K}{K!} e^{-\mu \mathcal{A}} \tag{1}$$

where $M(\mathcal{A})$ is the random variable representing the amount of users of a point process located in the area $\mathcal{A} \subset \mathbb{R}^2$ and μ (users/km^2) is the average user density per unit area. Since the process is homogeneous, μ is constant and it does not depend on the location. The K users generated from the Poisson process are conditionally independent and uniformly distributed in the circle, randomly deployed in circumferences with a certain distance ρ from BS given by $f_\rho(\rho) = 2\rho/R^2$. The azimuth angle ϕ inside the circle is generated via an uniform distribution between 0 and 2π. The UTs position is also composed by the z coordinate, i.e., the height h_{UT}, which is fixed at 1.5 m.

III. ARRAY PROCESSING

In this section the antenna array model and the antenna element pattern is described for both the BS and UT. We assume that the BS can be equipped either with a trisector antenna model, i.e., one UPA per sector, or with a UCyA covering the whole azimuthal range. The UT is modeled with 2 panels placed at the opposite sides of the terminal, each equipped with a UPA or a Uniform Linear Array (ULA). The positions of the BS and the UTs and the orientation of their arrays are defined in the Global Coordinate System (GCS), while antenna far-field patterns and polarization are given in the Local Coordinate System (LCS). The orientation of an array w.r.t. the GCS is defined in a sequence of rotations given by three angles: the bearing angle α, the down tilt angle β and the slant angle γ. We assume $\beta = \gamma = 0$ for both array types at the BS, while $\alpha = 0$ for UCyA and $\alpha = s120°$ for UPA with $s = -1, 0, 1$. For the UT, the orientation of the first panel w.r.t. the GCS is defined by:

$$\begin{aligned}
\alpha_{\text{UT}}^{(1)} &\sim \mathcal{U}(-180°, +180°) \\
\beta_{\text{UT}} &\sim \mathcal{N}(\mu_\beta, \sigma_\beta^2) \\
\gamma_{\text{UT}} &\sim \mathcal{N}(\mu_\gamma, \sigma_\gamma^2)
\end{aligned} \tag{2}$$

with $\mathcal{N}(\cdot)$ the continuous normal distribution, $\mu_\beta = \mu_\gamma = 0°$ and $\sigma_\beta^2 = \sigma_\gamma^2 = 36°$. Clearly, the second panel has the same β_{UT} and γ_{UT}, while $\alpha_{\text{UT}}^{(2)} = 180° + \alpha_{\text{UT}}^{(1)}$.

If we consider a point (x, y, z) in the unit sphere, defined as $\mathbf{r}(\theta, \phi) = [\sin\theta\cos\phi, \sin\theta\sin\phi, \cos\theta]^{\mathsf{T}}$ in Cartesian coordinates and this point represents a location in the GCS defined by θ and ϕ, the corresponding position in the LCS is given by $\mathbf{R}^{-1}\mathbf{r}$, where:

$$\mathbf{R} = \begin{pmatrix} \cos\alpha & -\sin\alpha & 0 \\ \sin\alpha & \cos\alpha & 0 \\ 0 & 0 & 1 \end{pmatrix} \begin{pmatrix} \cos\beta & 0 & \sin\beta \\ 0 & 1 & 0 \\ -\sin\beta & 0 & \cos\beta \end{pmatrix} \begin{pmatrix} \cos\alpha & -\sin\alpha & 0 \\ \sin\alpha & \cos\alpha & 0 \\ 0\alpha & 0 & 1 \end{pmatrix} \tag{3}$$

then, the transformations to obtain the azimuth angle ϕ' and zenith angle θ' in LCS are:

$$\theta'(\alpha, \beta, \gamma; \theta, \phi) = \arccos\left([0, 0, 1]\,\mathbf{R}^{-1}\mathbf{r}\right) \tag{4}$$

$$\phi'(\alpha, \beta, \gamma; \theta', \phi') = \arg\left([1, j, 0]\,\mathbf{R}^{-1}\mathbf{r}\right). \tag{5}$$

A. Antenna radiation pattern and polarization

The model and 3D radiation power pattern of each antenna element $A(\theta', \phi')$ is based on the Table 3 of ITU-R Recommendation M.2101 [13] and it is expressed in LCS, while the parameters for the BS are given by 3GPP TR 38.901 [7]: the angles corresponding to the Half Power Beamwidth (HPBW) are $\theta_{3\text{dB}} = \phi_{3\text{dB}} = 65°$, while $A_m = 30$ dB, where $-A_m$ is the minimum gain. The maximum directional gain of an antenna element $G_{\text{E,max}}$ is equal to 8 dBi. The parameters for the 3D radiation pattern of the UT antenna array element are based on 3GPP TR 38.803 [14]: $\theta_{3\text{dB}} = \phi_{3dB} = 90°$, $A_m = 25$ dB, $G_{\text{E,max}} = 5$ dBi.

The relation between the power pattern and the vertical and horizontal polarized field components in LCS, $F'_{\theta'}$ and $F'_{\phi'}$ respectively, is:

$$A'(\theta', \phi') = |F'_{\theta'}(\theta', \phi')|^2 + |F'_{\phi'}(\theta', \phi')|^2. \tag{6}$$

The definition of the two polarized field components depends on the polarization of the antenna elements. For single polarized antenna elements only the vertical polarized field component is active, so $F'_{\phi'} = 0$ and $F'_{\theta'} = \sqrt{A'(\theta', \phi')}$. In case of dual polarized antenna elements they can be expressed as:

$$F'_{\phi'} = \sqrt{A'(\theta', \phi')}\cos(\xi) \quad F'_{\phi'} = \sqrt{A'(\theta', \phi')}\sin(\xi) \tag{7}$$

where ξ is the polarization slant angle and $\xi = \pm 45°$ corresponds to a pair of cross polarized antenna elements. The transformation of the polarized field components from LCS to GCS is:

$$\begin{pmatrix} F_{rx,\theta}(\theta, \phi) \\ F_{rx,\phi}(\theta, \phi) \end{pmatrix} = \begin{pmatrix} +\cos\psi & -\sin\psi \\ +\sin\psi & +\cos\psi \end{pmatrix} \begin{pmatrix} F'_{rx\theta'}(\theta', \phi') \\ F'_{rx,\phi'}(\theta', \phi') \end{pmatrix} \tag{8}$$

where the angle ψ can be computed as:

$$\psi = \arg\begin{pmatrix} (\sin\gamma\cos\theta\sin(\phi - \alpha) + \\ \cos\gamma(\cos\beta\sin\theta - \sin\beta\cos\theta\cos(\phi - \alpha))) + \\ +j(\sin\gamma\cos(\phi - \alpha) + \sin\beta\cos\gamma\sin(\phi - \alpha)) \end{pmatrix}. \tag{9}$$

B. Uniform Planar Array (UPA)

The BS UPA for each sector is composed by a total of $N_t^{\text{UPA}} = N_{ty} \times N_{tz}$ antenna elements with the same polarization, where N_{ty} are the antennas along the y-axis and N_{tz} are the antennas along the z-axis. The UT arrays have $N_r = N_{ry} \times N_{rz}$ antenna elements. d_H and d_V are the distances, in horizontal and vertical direction respectively, for

$$\mathbf{H}_{u,v}^{\text{NLOS}} = \sum_{n=1}^{N_{\text{cl}}} \sum_{m=1}^{M_{\text{ray}}} \sqrt{\frac{P_n}{M_{\text{ray}}}} \begin{bmatrix} F_{rx,u}^{\theta}(\theta_{n,m}^{\text{ZoA}}, \phi_{n,m}^{\text{AoA}}) \\ F_{rx,u}^{\phi}(\theta_{n,m}^{\text{ZoA}}, \phi_{n,m}^{\text{AoA}}) \end{bmatrix}^{\mathsf{T}} \begin{bmatrix} e^{(j\Phi_{n,m}^{\theta\theta})} & \sqrt{\kappa_{n,m}^{-1}}e^{(j\Phi_{n,m}^{\theta\phi})} \\ \sqrt{\kappa_{n,m}^{-1}}e^{(j\Phi_{n,m}^{\phi\theta})} & e^{(j\Phi_{n,m}^{\phi\phi})} \end{bmatrix} \begin{bmatrix} F_{tx,v}^{\theta}(\theta_{n,m}^{\text{ZoD}}, \phi_{n,m}^{\text{AoD}}) \\ F_{tx,v}^{\phi}(\theta_{n,m}^{\text{ZoD}}, \phi_{n,m}^{\text{AoD}}) \end{bmatrix} [\mathbf{a}_{n,m}^{rx}]_u [\mathbf{a}_{n,m}^{tx}]_v \tag{10}$$

$$\mathbf{H}_{u,v}^{\text{LOS}} = \begin{bmatrix} F_{rx,u}^{\theta}(\theta_{\text{LOS}}^{\text{ZoA}}, \phi_{\text{LOS}}^{\text{AoA}}) \\ F_{rx,u}^{\phi}(\theta_{\text{LOS}}^{\text{ZoA}}, \phi_{\text{LOS}}^{\text{AoA}}) \end{bmatrix}^{\mathsf{T}} \begin{bmatrix} 1 & 0 \\ 0 & -1 \end{bmatrix} \begin{bmatrix} F_{tx,v}^{\theta}(\theta_{\text{LOS}}^{\text{ZoD}}, \phi_{\text{LOS}}^{\text{AoD}}) \\ F_{tx,v}^{\phi}(\theta_{\text{LOS}}^{\text{ZoD}}, \phi_{\text{LOS}}^{\text{AoD}}) \end{bmatrix} [\mathbf{a}_{\text{LOS}}^{rx}]_u [\mathbf{a}_{\text{LOS}}^{tx}]_v \tag{11}$$

the uniformly spaced antenna elements [15]. In our system, they are both equal to half the wavelength: $d_H = d_V = \lambda/2$, where $\lambda = c/f_c$ is the wavelength and c the speed of light. The index $s = (0, 1, 2)$ denotes the sector each array is assigned to. The UPA with $s = 0$ lies on the yz-plane (broadside to $\theta = 90°$, $\phi = 0°$), while the UPAs with $s = 1$ and $s = 2$ are broadside to $(\theta = 90°, \phi = 120°)$ and $(\theta = 90°, \phi = 240°)$, respectively.

The array factor can be found from the scalar product of the location matrix of the antenna elements $\mathbf{P}_{\text{UPA}}$ and the spherical unit vector $\mathbf{r}$ corresponding to the azimuth angle ϕ and zenith angle θ in GCS, given by the UT position:

$$\mathbf{a}(\theta, \phi) = \exp\left(\frac{j2\pi(\mathbf{P}_{\text{UPA}} \cdot \mathbf{r})}{\lambda}\right) \tag{12}$$

$\mathbf{P}_{\text{UPA}}$ is a $3 \times N_t^{\text{UPA}}$ matrix where each row corresponds to the position of the antenna elements along one of the three coordinates (x, y, z), rotated with respect the three rotation angles (α, β, γ), through the product with the rotation matrix $\mathbf{R}$:

$$\mathbf{P}_{\text{UPA}} = \mathbf{R}\left([\mathbf{0}_N, \text{vec}\left(\mathbf{d}_y \cdot \mathbf{1}_{N_{tz}}^{\mathsf{T}}\right), \text{vec}\left(\mathbf{1}_{N_{ty}} \cdot \mathbf{d}_z^{\mathsf{T}}\right)]\right)^{\mathsf{T}} \tag{13}$$

where the position vectors $\mathbf{d}_y$ and $\mathbf{d}_z$ are given by the relative positions of each antenna element along the y-axis and z-axis respectively:

$$\mathbf{d}_y = d_H [-N_y/2, \ldots, +N_y/2] \tag{14}$$
$$\mathbf{d}_z = d_V [-N_z/2, \ldots, +N_z/2] \tag{15}$$

vec$(\cdot)$ is the vectorization transformation, which concatenates the columns of a $N \times M$ matrix to produce a $NM \times 1$ column vector. The spherical unit vector $\mathbf{r}$ is obtained from the Zenith of Departure θ_{ZoD} and Azimuth of Departure ϕ_{AoD} for the transmitter, whereas the Zenith of Arrival θ_{ZoA} and Azimuth of Arrival ϕ_{AoA} for the receiver. Thus vector $\mathbf{r}$ becomes, respectively $\mathbf{r}_{tx} = \mathbf{r}(\theta_{\text{ZoD}}, \phi_{\text{AoD}})$ and $\mathbf{r}_{rx} = \mathbf{r}(\theta_{\text{ZoA}}, \phi_{\text{AoA}})$.

Finally, antenna array factor for the single element with index n_y along the y-axis and index n_z along the z-axis can be expressed as:

$$\exp\left(j2\pi/\lambda [d_H n_y \sin\theta \sin\phi + d_V n_z \cos\theta]\right).$$

C. Uniform Cylindrical Array (UCyA)

Regarding the array factor of the cylindrical array, it is defined as in (12), but the location matrix of the antenna array elements for the UCyA must take into account the different shape. Thus it is defined as:

$$\mathbf{P}_{\text{UCyA}} = \mathbf{R}\left[\text{vec}\left(\mathbf{d}_{u_x} \cdot \mathbf{1}_{N_z}^{\mathsf{T}}\right), \text{vec}\left(\mathbf{d}_{u_y} \cdot \mathbf{1}_{N_z}^{\mathsf{T}}\right), \text{vec}\left(\mathbf{1}_{N_c} \cdot \mathbf{d}_z^{\mathsf{T}}\right)\right]^{\mathsf{T}}. \tag{16}$$

In fact, an UCyA is composed by a certain number N_{tz} of rings (circles), each composed by N_{tc} elements uniformly placed along the circumference. The z-axis coordinate vector $\mathbf{d}_z$ is the same as for the UPA in (15), while $\mathbf{d}_{c_x}$ and $\mathbf{d}_{c_y}$ are the x and y coordinates of the antenna elements in each circle of radius R_c, given by:

$$\mathbf{d}_{c_x} = R_c \cos\left(2\pi/\lambda [0, \ldots, N_{tc} - 1]\right) \tag{17}$$
$$\mathbf{d}_{c_y} = R_c \sin\left(2\pi/\lambda [0, \ldots, N_{tc} - 1]\right). \tag{18}$$

The antenna factor for the single element with index n_c in the ring lying in the $x - y$ plane and index n_z of the ring z-coordinate can be expressed as:

$$\exp\left(j2\pi/\lambda [R_c \sin\theta \cos\left(\phi - 2\pi n_c/N_{tc}\right) + d_V n_z \cos\theta]\right).$$

The fairness of the comparison between the UCyA and UPA is guaranteed by taking $N_t^{\text{UCyA}} = N_{tc} \times N_{tz} = 3N_{ty} \times N_{tz}$.

IV. CHANNEL MODEL

To obtain reliable results from the system simulations, we adopt the latest 3GPP 3D stochastic channel model described in TR 38.901 [7]. It is designed for 5G mmWave massive MIMO communications, in the range 0.5-100 GHz. The propagation condition can be in Line of Sight (LOS) or Non-LOS (NLOS). According to the condition, each link experiences a different path loss, LOS probability and shadow fading. Moreover, the signal propagation is modeled as a superposition of different N_{cl} clusters, each one consisting of M_{ray} rays. Each cluster as its own parameters, such as direction of departure $(\phi_{\text{AoD}}, \theta_{\text{ZoD}})$ and direction of arrival $(\phi_{\text{AoA}}, \theta_{\text{ZoA}})$ in azimuth and zenith, and the cluster power P_n and cluster delay. A thorough description on how to generate all the involved channel parameters can be found in [7], [8]. For an OFDM subband, all cluster delays collapse into a single tap, therefore the MIMO flat channel matrix $\mathbf{H}_{u,v}^{\text{NLOS}}$ for the antenna element pair u at the receiver and v at the transmitter, can be computed as reported in (10). Where $[\mathbf{a}_{n,m}]_{u(v)}$ is the index u (v) of the array factor vector $\mathbf{a}(\theta_{n,m}^{\text{ZoA}} \phi_{n,m}^{\text{AoA}})$ for the receiver $(\mathbf{a}(\theta_{n,m}^{\text{ZoA}}, \phi_{n,m}^{\text{AoA}})$ for the transmitter). Moreover, $\{\Phi_{n,m}^{\theta\theta} \Phi_{n,m}^{\theta\phi} \Phi_{n,m}^{\phi\theta} \Phi_{n,m}^{\phi\phi}\}$ are the random initial phases for each ray m of each cluster n and for four different polarization combinations $(\theta\theta, \theta\phi, \phi\theta, \phi\phi)$, with distribution $\sim \mathcal{U}(-180°, +180°)$, and $\kappa_{n,m}$ is the cross polarization power ratios (XPR) for each ray m of each cluster n (7.5-21 in [7]). A realization of the main clusters and rays for a single BS-UT link can be represented as in Fig. 1, for the case of LOS link. For each cluster, only a single pair of BS-UT rays are reported.

For the LOS case the contribution of the main ray must be computed as in (11). Then the final $N_r \times N_t^{\text{UPA}}$ $(N_r \times N_t^{\text{UCyA}})$
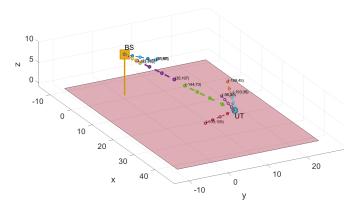
Figure 1: 3GPP spatial channel model. Representation of the 5 main clusters for a BS-UT link w.r.t. their powers and directions, in LOS.

matrix-valued channel impulse response for each BS sector and UT panel pair (for each UT panel) is given by the sum of the NLOS and LOS contributions:

$$\mathbf{H}^{\text{LOS}} = \sqrt{1/(K_R + 1)}\mathbf{H}^{\text{NLOS}} + \sqrt{K_R/(K_R + 1)}\mathbf{H}^{\text{LOS}} \quad (19)$$

where K_R is the Ricean factor.

V. MULTI-USER MULTI-LAYER MIMO SCHEME

Given the scenario illustrated in Sec. II, we assume that the BS transmits L data streams simultaneously to each UT, with $L \le N_r$ and $LK \le N_t$. We denote with $\mathbf{s}_k$ the $L \times 1$ data symbol vector to be transmitted to the k-th user, $\mathbb{E}[\mathbf{s}_k \mathbf{s}_k^H] = \frac{1}{L}\mathbf{I}$. At the BS, LK symbols $\mathbf{s} = [\mathbf{s}_1^\mathsf{T}, \mathbf{s}_2^\mathsf{T}, \ldots, \mathbf{s}_K^\mathsf{T}]^\mathsf{T}$ are precoded with a $N_t \times LK$ precoder $\mathbf{W} = [\mathbf{W}_1, \mathbf{W}_2, \ldots, \mathbf{W}_K]$ where $\mathbf{W}_k$ is the $N_t \times L$ precoder designed for user k. Furthermore, the following total power constraint $\|\mathbf{W}\|_F^2 \le P_{\text{tot}}$ is assumed, where P_{tot} denotes the transmitted power. The baseband equivalent receiving signal of the k-th user can be written as follows:

$$\mathbf{y}_k = \mathbf{H}_k \mathbf{x} = \mathbf{H}_k \sum_{i=1}^{K} \mathbf{W}_i \mathbf{s}_i + \mathbf{n}_k \quad (20)$$

where $\mathbf{n}_k \sim \mathcal{N}(0, \sigma_n^2 \mathbf{I})$ is a $N_r \times 1$ noise vector with independent and identically distributed entries, and σ_n^2 is the noise variance. We assume that $\mathbf{H}_k$ is the selected channel for user k with the highest energy among all 6 BS sector UT panel pairs in case of trisectorized UPAs (among the 2 UT panels in case of UCyA). Finally, ideal channel state information (CSI) at the BS is assumed and the BS resorts only to SDMA through precoding techniques, i.e., users communicate in the same time slot or resource and no user scheduling or clustering is performed.

A. Signal-to-Leakage-plus-Noise Ratio (SLNR) precoding

SLNR is a precoder scheme implemented at the transmitter for SDMA, that minimizes the interference caused by one user k to the others, denoted as the *leakage* [11]:

$$\sum_{i=1, \, i \ne k}^{K} \|\mathbf{H}_i \mathbf{W}_k\|_F^2 \quad (21)$$

where $\| \cdot \|_F^2$ is the Frobenius norm. The SLNR expression is the ratio between the signal power for user k and the noise plus the *leakage*:

$$\text{SLNR}_k = \frac{\|\mathbf{H}_k \mathbf{W}_k\|_F^2}{N_r \sigma_k^2 + \|\widetilde{\mathbf{H}}_k \mathbf{W}_k\|_F^2} \quad (22)$$

where:

$$\widetilde{\mathbf{H}}_k = [\mathbf{H}_1 \, \cdots \, \mathbf{H}_{k-1} \, \mathbf{H}_{k+1} \, \cdots \, \mathbf{H}_K]^\mathsf{T} \quad (23)$$

is an extended $N_r(K-1) \times N_t$ channel matrix that only excludes user k. It is shown in [16], [17] that the optimal precoder is linked to the solution of the generalized eigenvalue problem. Given $\mathbf{E} = [\mathbf{e}_1, \ldots, \mathbf{e}_{N_t}]$ the eigenvectors and $\mathbf{\Lambda} = \text{diag}([\lambda_1, \ldots, \lambda_{N_t}]^\mathsf{T})$ the eigenvalues of $\left(N_r \sigma_k^2 \mathbf{I} + \widetilde{\mathbf{H}}_k^H \widetilde{\mathbf{H}}_k\right)^{-1} \mathbf{H}_k^H \mathbf{H}_k$, the transmit precoding matrix targeted for user k that maximizes its SLNR is given by:

$$\mathbf{W}_k \propto [\mathbf{e}_1, \, \ldots, \, \mathbf{e}_L] \quad (24)$$

i.e., $\mathbf{W}_k$ is made by the L eigenvectors corresponding to the L largest eigenvalues $[\lambda_1, \, \ldots, \, \lambda_L]$.

B. MMSE combining

The combiner scheme is employed at each UT to minimize the intra-user inter-layer interference [12]. If we defined with $\mathbf{Z}_k = \mathbf{H}_k \mathbf{W}_k$ the equivalent channel matrix after precoding at the k-th user, we can design the $L \times N_r$ combining matrix $\mathbf{U}_k$, with L the number of layers, as a linear Minimum Mean Square Error (MMSE) receiver, defined as:

$$\mathbf{U}_k = \left(\mathbf{Z}_k^H \mathbf{Z}_k + \mathbf{G}_k\right)^{-1} \mathbf{Z}_k^H \quad (25)$$

with $\mathbf{G}_k$ the regularization matrix:

$$\mathbf{G}_k = \frac{\sigma^2}{P_{\text{tot}}}\mathbf{I} + \sum_{i=1, i \ne k}^{K}(\mathbf{H}_k \mathbf{W}_i)(\mathbf{H}_k \mathbf{W}_i)^H. \quad (26)$$

The estimated signal vector $\hat{\mathbf{s}}_k$ for UT k after MMSE combining becomes:

$$\hat{\mathbf{s}}_k = \mathbf{U}_k \mathbf{H}_k \sum_{i=1}^{K} \mathbf{W}_i \mathbf{s}_i + \mathbf{U}_k \mathbf{n}_k. \quad (27)$$

The total power P_{tot} is equally divided among the total KL streams. Finally, the SINR of layer l for user k is:

$$\text{SINR}_{k,l} = \frac{\left|\mathbf{u}_{k,l}^\mathsf{T} \mathbf{H}_k \mathbf{w}_{k,l}\right|^2}{\left\|\mathbf{u}_{k,l}^\mathsf{T}\right\|^2 \sigma_k^2 + \sum_{\substack{d=1 \\ d \ne l}}^{L} \eta_{k,d}^{k,l} + \sum_{\substack{i=1 \\ i \ne k}}^{K} \sum_{d=1}^{L} \eta_{i,d}^{k,l}} \quad (28)$$

where $\mathbf{u}_{k,l}^\mathsf{T}$ is the l-th row of matrix $\mathbf{U}_k$ and $\eta_{i,d}^{k,l} = \left|\mathbf{u}_{k,l}^\mathsf{T} \mathbf{H}_k \mathbf{w}_{i,d}\right|^2$ is the interfering term caused by layer d of user i on layer l of user k. The achievable rate in bps/Hz for user k can be computed as:

$$C_k = \sum_{l=1}^{L} \log_2(1 + \text{SINR}_{k,l}). \quad (29)$$

Table I: Main simulation parameters.

PARAMETER	VALUE
Carrier frequency f_c	28 GHz
Bandwidth B	50 MHz
Number of OFDM subcarriers Q	792
Subband	60 kHz
Noise figure F	7 dB
Maximum TX power $P_{tot,\text{UPA}}$	47 dBm
Maximum TX power $P_{tot,\text{UCyA}}$	51.8 dBm
Radius of the cell R	100 m
Network loading or user density μ	3500 users/km^2
Average number of UTs inside the cell	110 users
Polarization pol	single (dual)
Total antennas per BS UPA N_t^{UPA}	144 (288)
Total antennas per BS UCyA N_t^{UCyA}	432 (864)
Total antennas per UT N_r	2 (4)

Figure 3: CDF curves of rates for outdoor UTs in NLOS condition. For UCyA, $N_t^{UCyA} = 3N_{ty} \times N_{tz}$.

VI. RESULTS

In this section, we report the outcomes of our numerical simulations for a variety of configurations. Table I contains a list of the main system parameters.

In Figs. 2 and 3 we show the Cumulative Distribution Function (CDF) curves of the UT rate for different channel conditions and a variety of BS array configurations, number of layers and type of polarization ($pol = 1$ single, $pol = 2$ dual). Thus, different curves are obtained for outdoor UTs in LOS and outdoor UTs in NLOS. Please note that in case of dual polarization, the number of antennas is doubled at both the transmitter and the receiver w.r.t. single polarization. For UTs in LOS the results are show in Fig. 2. It can be appreciated how the UCyA array is outperforming the trisectorized UPA array in practically any case. The best transmitter configuration appears to be the 72×2, with dual polarized antenna elements and $L = 4$ layers. It can be remarked that the increase of the number of layers L allows some UTs to reach quite high rates, but it increases the rate standard deviation, i.e., the fairness among users is reduced. This can be seen from the steeper curves corresponding to
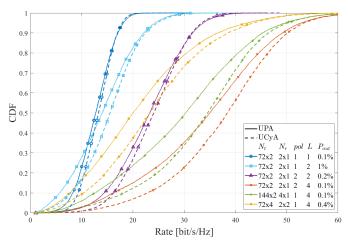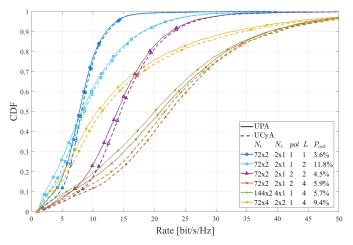
smaller number of layers, while a more smoother behaviour characterizes the curves with $L = 4$. In fact, the number of layers could produce an almost linear gain on the rate, but the increasing interference limits this improvement. In Fig. 3, for UTs in NLOS, the signal undergoes a harsher propagation condition, and this is clearly highlighted by the shift towards smaller rates of the CDF curves and the increased percentage of UTs in outage P_{out}, defined as the percentage of the UTs with $\frac{1}{L}\sum_{l=1}^{L}\text{SINR}_{k,l} < 0$ dB.

In Figs.4 and 5 we show the average rate of the UTs and their outage percentage as a function of all the possible antenna array configurations, i.e., we investigate on the distribution of antenna elements along the vertical axis and the horizontal axis for UPA (azimuthal plane for UCyA) by keeping constant the total number of transmitting antennas to $N_t^{\text{UPA}} = 144$ ($N_t^{\text{UCyA}} = 432$). The receiver array is set to 2×1, and both single and dual polarized antenna elements are considered, adopting respectively 2 and 4 layers. The results of these simulations can be seen in Fig. 4 and in Fig. 5 for UTs in LOS and NLOS condition respectively. The best performance clearly appears for configurations with larger number of antenna elements along the y-axis ($x - y$ plane). This could be explained by the fact that the UTs have the same height, therefore an increase of the beam resolution along the z-axis should not lead to any appreciable improvement. Finally, by comparing planar arrays (solid lines) against cylindrical arrays (dotted lines), these results confirm how the UCyA can guarantee better performance: about 5% improvement on the average rate and about 3% reduction on the outage.

VII. CONCLUSIONS

In this paper, we presented an analysis focused on the implementation of multi-user and multi-layer MIMO techniques with the latest 3GPP 3D channel model. It is of particular interest the comparison between the typical trisector cell site, adopting three planar arrays to cover each sector, and the implementation of a single cylindrical antenna array, able

Figure 2: CDF curves of rates for outdoor UTs in LOS condition. For UCyA, $N_t^{UCyA} = 3N_{ty} \times N_{tz}$.
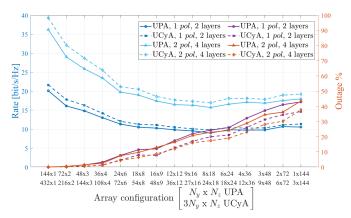
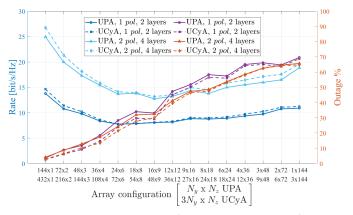Figure 4: Average per-user rate and outage vs. BS array configuration for outdoor UTs in LOS condition.

Figure 5: Average per-user rate and outage vs. BS array configuration for outdoor UTs in NLOS condition.

to cover the entire azimuthal range thanks to its particular shape. This second solution is able to outperform, in terms of achievable rate and experienced outage for the single UT, the UPA trisector solution. Future works will consider other interesting scenarios, such as indoor UTs in Urban Micro Street Canyon and Urban Macro, as well as outdoor UTs in Rural Macro scenario. Furthermore the main focus of future studies will be on user scheduling and clustering algorithms to further improve the interference reduction.

REFERENCES

[1] W. Roh, J.-Y. Seol, J. Park, B. Lee, J. Lee, Y. Kim, J. Cho, K. Cheun, and F. Aryanfar, "Millimeter-wave beamforming as an enabling technology for 5G cellular communications: theoretical feasibility and prototype results," *IEEE Communications Magazine*, vol. 52, no. 2, pp. 106–113, 2014.

[2] X. Gao, L. Dai, S. Han, C.-L. I, and R. W. Heath, "Energy-efficient hybrid analog and digital precoding for mmwave MIMO systems with large antenna arrays," *IEEE Journal on Selected Areas in Communications*, vol. 34, no. 4, pp. 998–1009, 2016.

[3] D. G. Riviello and R. Garello, "Implementation of 5G beamforming techniques on cylindrical arrays," in *2019 IEEE-APS Topical Conference on Antennas and Propagation in Wireless Communications (APWC)*, 2019, pp. 413–418.

[4] D. G. Riviello and F. D. Stasio, "5G beamforming implementation and trade-off investigation of cylindrical array arrangements," in *2019 22nd International Symposium on Wireless Personal Multimedia Communications (WPMC)*, 2019, pp. 1–6.

[5] N. Wu, F. Zhu, and Q. Liang, "Evaluating spatial resolution and channel capacity of sparse cylindrical arrays for massive MIMO," *IEEE Access*, vol. 5, pp. 23 994–24 003, 2017.

[6] M. Kurras, Y. Miao, L. Thiele, S. Varatharaajan, N. Hadaschik, M. Grossmann, and M. Landmann, "On the application of cylindrical arrays for massive MIMO in cellular systems," in *WSA 2018; 22nd International ITG Workshop on Smart Antennas*, 2018, pp. 1–8.

[7] 3GPP, "Study on channel model for frequencies from 0.5 to 100 GHz (release 16) v16.1.0," Tech. Rep., 2020, 3GPP, Sophia Antipolis, France, Rep. TR 38.901.

[8] D. G. Riviello, F. Di Stasio, and R. Tuninato, "Performance analysis of multi-user MIMO schemes under realistic 3GPP 3-D channel model for 5G mmwave cellular networks," *Electronics*, vol. 11, no. 3, 2022. [Online]. Available: https://www.mdpi.com/2079-9292/11/3/330

[9] Q. Spencer, A. Swindlehurst, and M. Haardt, "Zero-forcing methods for downlink spatial multiplexing in multiuser MIMO channels," *IEEE Transactions on Signal Processing*, vol. 52, no. 2, pp. 461–471, 2004.

[10] D. H. Nguyen and L.-N. Tho, "MMSE precoding for multiuser MISO downlink transmission with non-homogeneous user SNR conditions," *EURASIP Journal on Advances in Signal Processing*, vol. 2014, no. 85, 2014.

[11] A. Tarighat, M. Sadek, and A. Sayed, "A multi user beamforming scheme for downlink MIMO channels based on maximizing signal-to-leakage ratios," in *Proceedings. (ICASSP '05). IEEE International Conference on Acoustics, Speech, and Signal Processing, 2005*, vol. 3, 2005, pp. iii/1129–iii/1132 Vol. 3.

[12] N. Kim, Y. Lee, and H. Park, "Performance analysis of MIMO system with linear MMSE receiver," *IEEE Transactions on Wireless Communications*, vol. 7, no. 11, pp. 4474–4478, 2008.

[13] I.-R. R. S. of ITU, "Modelling and simulation of IMT networks and systems for use in sharing and compatibility studies (m.2101-0)," Tech. Rep., Feb. 2017, 3GPP, Sophia Antipolis, France, Rep. TR 38.901.

[14] 3GPP, "Study on new radio access technology: Radio frequency (RF) and co-existence aspects v14.2.0," Tech. Rep., 2017, 3GPP, Sophia Antipolis, France, Rep. TR 38.803.

[15] Q.-U.-A. Nadeem, A. Kammoun, M. Debbah, and M.-S. Alouini, "Design of 5G full dimension massive MIMO systems," *IEEE Transactions on Communications*, vol. 66, no. 2, pp. 726–740, 2018.

[16] M. Sadek, A. Tarighat, and A. H. Sayed, "Active antenna selection in multiuser MIMO communications," *IEEE Transactions on Signal Processing*, vol. 55, no. 4, pp. 1498–1510, 2007.

[17] B. Ren, M. Wang, C. Yang, L. Wang, J. Zou, T. Liu, and W. Yang, "An improved leakage-based precoding scheme for multi-user MIMO systems," in *2013 IEEE 77th Vehicular Technology Conference (VTC Spring)*, 2013, pp. 1–4.